

# $\delta$ Ceti is not monoperiodic: seismic modeling of a $\beta$ Cephei star from MOST<sup>1</sup> spacebased photometry

C. Aerts<sup>2,3</sup>, S.V. Marchenko<sup>4</sup>, J.M. Matthews<sup>5</sup>, R. Kuschnig<sup>5</sup>, D.B. Guenther<sup>6</sup>, A.F.J. Moffat<sup>7</sup>, S.M. Rucinski<sup>8</sup>, D. Sasselov<sup>9</sup>, G.A.H. Walker<sup>10</sup>, and W.W. Weiss<sup>11</sup>

## ABSTRACT

The  $\beta$  Cephei star  $\delta$  Ceti was considered one of the few monoperiodic variables in the class. Despite (or perhaps because of) its apparently simple oscillation spectrum, it has been challenging and controversial to identify this star's pulsation mode and constrain its physical parameters seismically. Broadband time-resolved photometry of  $\delta$  Ceti spanning 18.7 days with a duty cycle of about 65% obtained by the MOST (Microvariability & Oscillations of STars) satellite – the first scientific observations ever obtained by MOST – reveals that the star is actually multiperiodic. Besides the well-known dominant frequency of  $f_1 = 6.205886$  d<sup>-1</sup>, we have discovered in the MOST data its first harmonic  $2f_1$  and three other

---

<sup>1</sup> Based on data from the MOST satellite, a Canadian Space Agency mission, jointly operated by Dynacon Inc., the University of Toronto Institute for Aerospace Studies and the University of British Columbia, with the assistance of the University of Vienna.

<sup>2</sup>Institute of Astronomy, University of Leuven, Celestijnenlaan 200 B, B-3001 Leuven, Belgium, email: conny@ster.kuleuven.be

<sup>3</sup>Department of Astrophysics, Radboud University Nijmegen, P.O. Box 9010, 6500 GL Nijmegen, the Netherlands

<sup>4</sup>Department of Physics and Astronomy, Western Kentucky University 1906 College Heights Blvd 11077, Bowling Green, KY 42101-1077, USA

<sup>5</sup>Department of Physics and Astronomy, University of British Columbia, 6224 Agricultural Road, Vancouver, BC V6T 1Z1, Canada

<sup>6</sup> Department of Astronomy and Physics, St. Mary's University, Halifax, NS B3H 3C3, Canada

<sup>7</sup>Département de Physique, Université de Montréal, C.P. 6128, Succursale Centre-Ville, Montréal, QC H3C 3J7, Canada

<sup>8</sup>David Dunlap Observatory, University of Toronto, P.O. Box 360, Richmond Hill, ON L4C 4Y6, Canada

<sup>9</sup>Harvard-Smithsonian Center for Astrophysics, 60 Garden Street, Cambridge, MA 02138, USA

<sup>10</sup>1234 Hewlett Place, Victoria, BC V8S 4P7, Canada

<sup>11</sup>Institut für Astronomie, Universität Wien, Türkenschanzstrasse 17, A-1180 Wien, Austria

frequencies ( $f_2 = 3.737 \text{ d}^{-1}$ ,  $f_3 = 3.673 \text{ d}^{-1}$  and  $f_4 = 0.318 \text{ d}^{-1}$ ), all detected with  $S/N > 4$ . In retrospect,  $f_2$  was also present in archival spectral line profile data but at lower  $S/N$ . We present seismic models whose modes match exactly the frequencies  $f_1$  and  $f_2$ . Only one model falls within the common part of the error boxes of the star’s observed surface gravity and effective temperature from photometry and spectroscopy. In this model,  $f_1$  is the radial ( $\ell = 0$ ) first overtone and  $f_2$  is the  $g_2$  ( $\ell = 2$ ,  $m = 0$ ) mode. This model has a mass of  $10.2 \pm 0.2 M_\odot$  and an age of  $17.9 \pm 0.3$  million years, making  $\delta$  Ceti an evolved  $\beta$  Cephei star. If  $f_2$  and  $f_3$  are rotationally split components of the same  $g_2$  mode, then the star’s equatorial rotation velocity is either  $27.6 \text{ km s}^{-1}$  or half this value. Given its  $v \sin i$  of about  $1 \text{ km s}^{-1}$ , this implies we are seeing  $\delta$  Ceti nearly pole-on.

*Subject headings:* stars: early-type; stars: individual (HD 16582); stars: oscillations; stars:  $\beta$  Cephei

## 1. Introduction

Asteroseismic modeling of  $\beta$  Cephei pulsators offers an important window on the structure and evolution of massive evolved B stars which are precursors to core-collapse supernovae. Significant progress has been made recently thanks to groundbased single-site photometric campaigns lasting many years and multi-site synoptic campaigns lasting several months. The first method made possible the identification of 6 pulsation modes in HD 129929 (B3V), leading to the first observational proof of non-rigid rotation inside a star other than the Sun (Aerts et al. 2003). The second method resulted in the identification of about 20 frequencies in the star  $\nu$  Eri (B2III, Handler et al. 2004, Aerts et al. 2004, De Ridder et al. 2004) and a second strong case for differential internal rotation (Pamyatnykh et al. 2004) in a massive B star. These successes have prompted similar studies of other  $\beta$  Cephei stars; e.g.,  $\theta$  Oph (B2IV, Handler et al. 2005; Briquet et al. 2005) and 12 Lac (B2III, Handler et al. 2006). Photometry from a spacebased platform offers the advantages of both methods, producing long time series of much higher duty cycles than are possible from the ground. This paper is an indication of what is possible when such data become available for even a seemingly simple  $\beta$  Cephei star which has been investigated for decades with only limited progress.

The bright star  $\delta$  Ceti ( $m_V = 4.07$ , B2IV) is one of the very few  $\beta$  Cephei stars thought to be a monoprotic pulsator within that class (Stankov & Handler 2005 and references therein). Its variability has been investigated in a number of ground-based studies, most of which were based on only a few nights of data. A clear overview of these studies up to

1987 is not repeated here since it can be found already in Jerzykiewicz et al. (1988), who investigated the star’s behaviour from multicolor photometry taken during seven consecutive nights in 1981 and one night in 1982, as well as from archival data. These authors put forward one oscillation frequency equal to  $6.20587545 \text{ d}^{-1}$  with an amplitude of  $\approx 12 \text{ mmag}$  from data assembled between 1963 and 1982. From their new data, they found night-to-night variations of the mean brightness and of the amplitude in the *uvby* filters. They attributed the amplitude variability to either a secondary short period with an amplitude below  $1.6 \text{ mmag}$  or a slow drift in the data, or both. They did not find any night-to-night phase variations.

Kubiak & Seggewiss (1990) collected 2 nights of simultaneous spectroscopic and photo-electric observations of the star and confirmed the phase lag between the radial velocity and light curves of 0.23 found in earlier studies.

Aerts et al. (1992) discovered large-amplitude line-profile variations in  $\delta$  Ceti, from which they identified the single frequency as a radial mode with a velocity amplitude of  $7.4 \pm 0.1 \text{ km s}^{-1}$ . This identification was confirmed from available multicolor photometry by Cugier et al. (1994) and by Cugier & Nowak (1997).

Finally, Daszyńska-Daszkiewicz et al. (2005) tried to put constraints on the internal physics of the star and to identify the radial order of the mode from combined multicolor photometry and radial-velocity data. They found significant differences between the data and their seismic models depending on whether they adopted OPAL or OP opacities, and could not conclude definitely if  $\delta$  Ceti was pulsating in the radial fundamental or first overtone mode. Neither model scenario could be made to agree with the observations.

New space-based observations of  $\delta$  Ceti by the MOST satellite have now provided key clues to understanding this star. The first ground-based observations of  $\delta$  Ceti were obtained over a century ago, and over the course of the last three to four decades, there has been a prolonged debate about its amplitude modulation, possible multiperiodicity and period changes. In that time, a grand total of about 30 cycles of its dominant pulsation mode have been monitored. In less than three weeks, MOST was able to thoroughly sample over 70 cycles.

## 2. Observations and data reduction

The MOST (Microvariability & Oscillations of STars) satellite (Walker, Matthews et al. 2003), housing a 15-cm Rumak-Maksutov optical telescope feeding a CCD photometer, was launched in June 2003. Its primary mission is ultraprecise rapid photometry for astero-

seismology. MOST was designed to monitor stars at a rate as high as 10 times per minute with a single-point precision of about 1-2 millimag. For stars within the satellite’s Continuous Viewing Zone (CVZ) – in a declination range  $-18^\circ \leq \delta \leq +36^\circ$  – data can be collected nearly without interruption for up to 8 weeks. The combination of single-point precision, and long time coverage with high duty cycle, leads to sensitivity to rapid oscillations in Fourier space as low as about  $1 \mu\text{mag} = 1 \text{ part per million (ppm)}$ . An example of the photometric precision can be seen in Matthews et al. (2004).

During the early stages of the mission when MOST was being checked out for routine scientific operations, the MOST Team decided to use  $\delta$  Ceti (conveniently located in the CVZ) as its first test target, for what was designated Commissioning Science. At the time of the  $\delta$  Ceti observations – the first scientific data collected by MOST – the spacecraft pointing had not yet been optimised, debugging of onboard software led to computer crashes which introduced gaps into the time series, and the downlink to Earth did not yet permit the nominal science data sampling rate. Hence, the photometric precision and duty cycle were far from what MOST was capable of achieving once commissioning was complete. However, at the time, this light curve represented the best combination of precision, duration and duty cycle ever obtained for any astronomical object other than the Sun.

MOST monitored  $\delta$  Ceti for 18.68 days during 08 - 27 October 2003, with 10-s exposures at a sampling interval of 120 s. The data were obtained through a broadband filter designed expressly for the MOST instrument, with a bandpass of about 350–700 nm and a throughput approximately  $3\times$  that of a Johnson V filter. The data were reduced independently by two of the authors (SM and RK), yielding similar results. We present here the SM reduction, described below.

The principal observing mode for MOST is known as Fabry Imaging, in which the light from a bright star illuminates a Fabry microlens which projects an image of the telescope pupil onto the CCD (see Walker, Matthews et al. 2003, and their Fig. 10). The star is centred in a field stop 1 arcmin in diameter, and the doughnut-shaped pupil image covers about 1300 pixels in a square CCD subraster of 58 pixels on a side. Seven adjacent Fabry microlenses sample the surrounding sky background. (One neighbouring lens is not used because its reading is contaminated by light from the star as pixels are transferred under the Target Star beam during readout.)

Data are returned to Earth in two formats, or Science Data Streams, known as SDS1 and SDS2. The former is processed on board so that only a small set of integrated numbers is sent to Earth; the latter consists of resolved Fabry images which can be fully reduced on the ground. Because of the limitations of the commissioning performance, the quality of the SDS1 data (numbering about 10,000) were severely compromised and are not used for this

reduction. The Fabry images of the  $\delta$  Ceti SDS2 data were binned  $2 \times 2$  to form a  $29 \times 29$  pixel image. For each image, all the available estimates of biases were iteratively checked for significant outliers and, using appropriate weights, combined to provide an average for a given image.

Most of the data reduction effort is made to correct for the changing background, primarily due to orbital modulation of scattered Earthshine. Detailed aspects of this stray light are described by Reegen et al. (2005). Readings from the 7 adjacent Fabry microlenses (after  $3\sigma$ -clipping of outliers) were used to derive unweighted averages of the background. The Primary Target Fabry field also contains about 350 pixels with only background that were used to calculate a third background average. This last estimate of the background turned out to give the best removal of stray light artifacts, and it alone was used for the current reduction.

Since  $\delta$  Ceti was observed during satellite commissioning, and the pointing accuracy was still far from optimal, the pointing errors (with  $\sigma_{X,Y} \sim 1$  pixel) were tracked for each exposure, based on the ACS (Attitude Control System) telemetry. The pointing errors (and other possible inhomogeneities in the optics) were also estimated directly from the images themselves by comparing the average fluxes in the four image quadrants. Large deviations from quadrant to quadrant were flagged and could lead to rejection of an image.

After bias and background subtraction, each Fabry target image was assigned a quality rank. This was calculated by adding ‘penalties’ and rejecting all images with a penalty count exceeding 3. Any large deviation ( $> 3.5\sigma$  above average) in the X or Y pointing of the satellite (updated once per second) added 1 to the penalty count. A similarly large deviation of the  $(X^2 + Y^2)$  pointing vector, as well as an excessive number of  $> 3.5\sigma$  shifts from the average position in a 10-sec exposure (more than 3 such deviations in a set of 10 successive readings) added 1.5 each to the penalty. Any large systematic shift ( $> 5$  pixels, either in X or Y) of the 10-sec average from the global average position from the entire run resulted in immediate rejection of the image. The rest of the quality ranking was based on dividing each Fabry image into four quadrants and assessing the uniformity across these quadrants. An iterative calculation of the percentage of outlying pixels in each quadrant (usually due to cosmic ray strikes or hot pixels in the CCD) sets the next component of the rank. If the number of rejected pixels exceeded 5% or 10%, the penalty was increased by 1 or 2, respectively. An image was rejected if any single quadrant contained more than 50% of the total number of faulty pixels (even if that number was below 10%), or any combination of 2 quadrants was responsible for 75% of the bad pixels.

The pre-selected pixels in each image which passed the quality control were added to produce an instrumental flux value. The instrument telemetry also includes the CCD focal

plane temperature, which was not completely regulated during the commissioning observations. Correlations between CCD temperature and the image fluxes were corrected. The final stage of the reduction was high-pass filtering and  $3\sigma$ -clipping of the data to remove any rapid changes in stray light that survived the earlier quality tests. For the period range of relevance for  $\delta$  Ceti, this is not expected to remove any intrinsic stellar signal. As a reality check, we always compared the corrected fluxes to the original raw estimates. Any large deviations ( $\delta m \geq 0.005$  mag) were re-examined to avoid the danger of spurious overcorrection.

The duty cycle of the original SDS1 + SDS2 photometry was about 65%, with a stretch of 11 days reaching about 95%. The exclusion of the SDS1 data, and the data rejection above, reduces the total number of data points from 3267 to 2949. The absolute duty cycle of this filtered light curve is only 22%, but it should be noted the reduction in duty cycle is primarily in each orbital cycle of 101.4 min, with no regular daily gaps as in groundbased photometry. The overall sampling of the  $\delta$  Ceti light curve still approaches a duty cycle of 65%.

The total standard deviation of the 2949 data point set is 8.47 mmag, which is dominated by the intrinsic pulsational variability of the star. The phase diagram of the data, folded at the known dominant pulsation period, is presented in Fig. 1. This plot, and the light curve segments shown in Fig. 6, illustrate the thorough coverage and quality of the MOST photometry of  $\delta$  Ceti.

### 3. Data analysis

#### 3.1. Discovery of the multiperiodicity of $\delta$ Ceti

We computed the Scargle Fourier periodogram (Scargle 1982) of the data (Fig. 2b) with a sampling of  $10^{-6}$  d $^{-1}$  and found the expected dominant peak at  $f_1 = 6.20589(8)$  d $^{-1}$  ( $= 71.827$   $\mu$ Hz);  $P = 0.16114$  d  $= 3.867$  hr. The error estimate of  $8 \times 10^{-5}$  d $^{-1}$  was computed as  $\sigma_f = \sqrt{6} \sigma_{\text{std}} / \pi \sqrt{N} A \Delta T$  (Montgomery & O’Donohue & 1999), with  $N$  the number of measurements,  $A$  the amplitude,  $\Delta T$  the total time span and  $\sigma_{\text{std}}$  the standard deviation of the final residuals. This value of  $f_1$  is identical to within the errors, to the value reported by Jerzykiewicz et al. (1988). We then compared the periodogram to the spectral window function (Fig. 2a), which was computed from a sinusoid of the same frequency and amplitude as peak  $f_1$  sampled at the same times as the real time series.

A least-squares harmonic fit to the data, fixing the value of  $f_1$  above, gives an amplitude for that peak of 11.62(3) mmag, and reveals the presence of the first harmonic  $2f_1$  with an amplitude of 0.72(3) mmag and a signal-to-noise of about  $7.5\sigma$ . While harmonics of principal

oscillation frequencies have been found in other  $\beta$  Cephei stars (e.g., Heynderickx et al. 1994), one was never before detected in  $\delta$  Ceti. This is not surprising given its amplitude is only 6% of that of  $f_1$ .

Subtracting  $f_1$  and  $2f_1$  from the data results in the periodogram shown in Fig. 2c. The overall variance of the time series has been reduced by 96.6%, so the residuals have a standard deviation of only  $\sigma = 1.56$  mmag. Four peaks are immediately obvious in Fig. 2c: 0.02, 2.00, 3.73, and 14.20  $\text{d}^{-1}$ . The last corresponds to the known orbital frequency of the MOST satellite, and is an observed artifact in later MOST data, due to the modulation of scattered Earthshine in the MOST focal plane with the orbital period. The 2.00  $\text{d}^{-1}$  frequency is also almost certainly an artifact. It is due to a modulation of the stray light from the Earth as MOST’s Sun-synchronous dusk-dawn orbit takes it over similar features of the Earth’s albedo on a daily cycle. In this case, it may be due to the maxima in the Earth’s albedo near both poles, not long after the Autumnal Equinox.

The low-frequency peak near 0.02  $\text{d}^{-1}$  is consistent with a long-term trend in the data, discussed below. The remaining peak, labeled  $f_2$  in Fig. 2c, cannot be ascribed to any known instrumental artifact and is almost certainly intrinsic to  $\delta$  Ceti.

### 3.2. Long-term variability

In its Fabry Imaging mode, MOST is a non-differential experiment, with no comparison star observed in a comparable fashion in the field. However, experience with 2 years of MOST data has shown that the instrument is remarkably stable. Because of the previous observation by Jerzykiewicz et al. (1988) of a monotonic amplitude change over 7 consecutive nights, and the presence of a low-frequency peak in Fig. 2c, we searched for evidence of such amplitude changes before proceeding with frequency analysis of the MOST photometry.

We divided the time series into subsets. Each subset was longer than the dominant period of 0.17 d but shorter than 0.5 d so as to mimic the previous ground-based data. Each subset used had at least 50 data points and no large gaps. We produced 25 such subsets and fitted them with  $f_1$  and  $2f_1$ , allowing the amplitudes and phases to be free parameters. The resulting amplitudes, phases and “nightly” means of  $f_1$  are plotted in Fig. 3.

All three quantities vary beyond the error bars of the individual points, but in a complicated fashion. However, the total ranges of variability are small: about 15% in amplitude, 4% in phase, and about 0.4% in mean brightness. The mean brightness does show the clearest evidence for a trend, which turns out to be responsible for the peak near 0.02  $\text{d}^{-1}$  ( $P \sim 50$  d).

We then fitted the data residuals from Sect. 3.1 ( $f_1$  and  $2f_1$  prewhitened) with a linear trend as shown in Fig. 4. The linear fit corresponds to a brightness increase of  $0.154 \text{ mmag/day} = 0.0064 \text{ mmag/hour}$ . This is more than 2 orders of magnitude smaller than the trend of about  $1 \text{ mmag/hour}$  reported by Jerzykiewicz et al. (1988) in their Strömgren photometry of  $\delta$  Ceti.

We cannot confirm whether the trend seen by MOST is stellar or instrumental (see discussion in Sect. 5) but we nonetheless remove it from the data for subsequent analysis. The detrended residuals have a standard deviation of  $1.37 \text{ mmag}$ ,  $0.19 \text{ mmag}$  smaller than before.

### 3.3. Additional oscillation frequencies in $\delta$ Ceti

Removing the trend from the data presented in Fig. 4 produced the periodogram shown in Fig. 5a. Not surprisingly, the peak at  $0.02 \text{ d}^{-1}$  vanished. Perhaps surprisingly, the peak at  $14.2 \text{ d}^{-1}$  also disappeared. It turned out not to be due primarily to modulated stray Earthshine but to the long-term trend sampled with gaps in the data at the orbital frequency (due to outages during the spacecraft commissioning phase).

The peak at  $2.003 \text{ d}^{-1}$  does remain, consistent with a genuine stray light artifact, although its amplitude has been reduced by more than half, so the trend contributed to it as well.

The frequency  $f_2 = 3.737(2) \text{ d}^{-1}$  persists as well, and its amplitude of  $0.53(3) \text{ mmag}$  – significant at the  $5.6\sigma$  level – is almost unchanged from the original data before the trend was removed. We note that this frequency and the dominant frequency  $f_1$  have a beat period  $1/(f_1 - f_2) = 0.405 \text{ d} \sim 9.7 \text{ hr}$ , which is well sampled by several continuous stretches in the MOST time series but not by the nightly stretches in the groundbased data of Jerzykiewicz et al. (1988).

Prewhitening the MOST residuals by frequency  $f_2$  and the artifact at  $2.003 \text{ d}^{-1}$  reduces the standard deviation by  $0.12 \text{ mmag}$  to  $1.25 \text{ mmag}$ . From these residuals, we obtain the periodogram plotted in Fig. 5b. This contains two peaks with significance greater than  $4\sigma$ , namely  $f_3 = 3.673(2) \text{ d}^{-1}$  and  $f_4 = 0.318(2) \text{ d}^{-1}$ , with amplitudes of  $0.39(4) (4.0\sigma)$  and  $0.43(4) \text{ mmag} (4.5\sigma)$ , respectively.

Prewhitening the data by these two additional frequencies reduces the overall  $\sigma$  by only  $0.07 \text{ mmag}$ . A plot of the final residuals is given in Fig. 7 and their periodogram is shown in Fig. 5c.



There are peaks with amplitudes below 0.4 mmag which may help account for the complex amplitude and phase behaviour seen in Fig. 3. These include a peak at  $3.909(5) \text{ d}^{-1}$  at the  $3.5\sigma$  level, and one at  $3.805(6) \text{ d}^{-1}$  at the  $2.8\sigma$  level.

### 3.4. Reexamination of archival data

In light of this frequency analysis of the MOST data, we reanalysed two high-precision archival data sets of  $\delta$  Ceti:

1. the HIPPARCOS light curve (Perryman et al. 1997), consisting of 72 data points covering 1096 days with a quasi-equidistant spacing of about 15 days; and
2. the 60 moment variations derived from single-site high-resolution line-profile observations by Aerts et al. (1992), spanning 7 days.

Neither of these data sets showed any significant long-term trends. After prewhitening both independent data sets with frequency  $f_1$ , we searched for evidence of  $f_2$  in the residuals. There was no sign of signal at  $f_2$  in the HIPPARCOS photometry, which is not surprising given its low amplitude in the MOST data and the poor sampling of the HIPPARCOS data for this relatively short period. However, in a periodogram of the first velocity moment  $\langle v \rangle$  computed by Aerts et al. (1992) from their line-profile data, a peak shows up near  $f_2$ , with an amplitude of  $0.27 \pm 0.09 \text{ km s}^{-1}$ , corresponding to a significance of only  $3\sigma$ . Despite the low significance, and because of its presence in the MOST data, we conducted a second investigation of  $f_2$  in the archival data.

The dominant frequency  $f_1$  is present in the HIPPARCOS data with a comparable amplitude to that seen in the MOST data, despite the use of different custom filters for these observations. So we prewhitened the HIPPARCOS and MOST (detrended) lightcurves and the  $\langle v \rangle$  moment data by  $f_1$  and  $2f_1$ , and then normalised the resulting Scargle periodograms to the highest peak in each. We then multiplied these normalised periodograms together, with the logic that if  $f_2$  (or any other common frequency) was present in more than one of the data sets, it would show up with improved  $S/N$  over the MOST data alone. If  $f_2$  was absent in the other sets, it would reduce the  $S/N$  over MOST alone. In this exercise, all three data sets were given equal weight.

The outcome is shown in Fig. 5c. Two peaks are immediately obvious to the eye; at  $f_2$  and  $2.00 \text{ d}^{-1}$ . The latter has been reduced in significance, consistent with it being an artifact in the MOST data alone, while  $f_2$  now has a significantly higher  $S/N$  of 8.6. Closer examination (and prewhitening) reveals the presence of a third peak at  $f_3$  at the  $4.6\sigma$  level,

higher than in the MOST data alone. The frequency  $f_4$  is not evident in the combined normalised periodogram.

These results lend circumstantial support to the presence of the frequencies  $f_2$  and  $f_3$  in one or both of the HIPPARCOS and line-profile data sets, with the *a posteriori* knowledge from the MOST photometry.

### 3.5. Solution to the MOST light curve

The final fit which we applied to the MOST light curve is as follows:

$$y_i = a + bt_i + \sum_{j=1}^6 c_j \sin[2\pi(f_j t_i + \phi_j)], \quad (1)$$

with the parameters provided in Table 1. We have retained only frequencies with amplitudes of significance  $\geq 4.0\sigma$ , following the acceptance criterion proposed by Breger et al. (1993) and Kuschnig et al. (1997).

Two segments of the light curve comparing this solution to the data are shown in Fig. 6. The full line corresponds to Equation (1), while the dotted line is a solution including only the linear trend and the dominant frequency  $f_1$ . The residuals for the two solutions are shown in Fig. 7, at a magnified vertical scale. In particular, the full solution does a much better job near the well-populated minima and maxima of the light curve and leads to smaller residuals.

## 4. Seismic interpretation

### 4.1. Fitting $f_1$ and $f_2$

To compare the oscillation frequencies we have detected in  $\delta$  Ceti with those predicted by pulsational models of B-type stars, we explored the database described by Ausseloos et al. (2004). This database contains evolutionary models from the ZAMS to the turnoff with masses ranging from 7 to 13  $M_\odot$  (in steps of  $0.1M_\odot$ ),  $X$  fixed at 0.70,  $Z$  ranging from 0.012 to 0.030 (in steps of 0.002), and three choices for the core overshoot parameter ( $\alpha_{\text{ov}} = 0.0, 0.1$  or  $0.2$ ). For a description of the input physics of these models, and the computation of their oscillation frequencies, we refer to Ausseloos et al. (2004).

Since analyses of the line-profile variations and earlier multicolor photometry indicate that the dominant pulsation frequency  $f_1$  corresponds to a radial mode (Aerts et al. 1992;

Cugier et al. 1994), we have restricted our search of the model grid to those models with radial modes which coincide with  $f_1$ . We have further constrained the search by forcing  $f_2$  to correspond to zonal modes of  $\ell_2 = 0, 1$  or  $2$ , using the fitting algorithms of Ausseloos (2005). Modes with  $\ell \geq 3$  are unlikely to be observed in integrated photometry due to cancellation effects across the stellar disk. The assumption of non-zonal modes ( $m \neq 0$ ) is considered safe since  $\delta$  Ceti has a low projected rotational velocity ( $v \sin i \sim 1 \text{ km s}^{-1}$ ; Aerts et al. 1992) so even a non-zero  $m$  component of mode  $f_2$  should lie close to the central component of the multiplet. (See our discussion in Sect. 4.2 about the inferred rotational velocity of  $\delta$  Ceti and the validity of this assumption.)

There are no models in the database which are consistent with both  $f_1$  and  $f_2$  being radial ( $\ell = 0$ ) modes. We found 66 models which satisfy the criteria that  $f_1$  is a radial mode and  $f_2$  is an  $\ell = 1$  or  $2$  mode; 40 models for the former, and 26 for the latter. All the models fitting  $f_1$  and  $f_2$  simultaneously are indicated in the theoretical ( $\log T_{\text{eff}}, \log g$ ) diagram shown in Fig. 8.

We also have independent empirical constraints on the position of  $\delta$  Ceti in Fig. 8. We plot the star’s empirical error box derived from photometric colors averaged over the dominant pulsation cycle in three different systems (Walraven, Geneva and Strömgren) as determined by Heynderickx et al. (1994). We also show the spectroscopic error box recently derived by Morel et al. (private communication) based on high-resolution échelle spectra covering the whole pulsation cycle. We prefer this over previous estimates relying on a single spectrum during the cycle (e.g., Gies & Lambert 1994). We put more weight on the photometric error box due to its smaller extent, and the fact that it is based on three different photometric systems.

It can be seen in Fig. 8 that the majority of the models matching both  $f_1$  and  $f_2$  are too evolved (i.e., have too low gravities) for the photometric and spectroscopic error boxes. In fact, only five models fall within the photometric box; their physical characteristics are listed in Table 2. The non-radial mode corresponding to  $f_2$  is the  $g_2$  mode for all of these models. All these models require some amount of core overshooting.

Which of these models is most likely to be excited? We checked the excitation rates with the non-adiabatic code MAD (Dupret 2001) and found that the radial first overtone of Model 1 in Table 2 (shown as “o” in Fig. 8) is expected to be stable due to its low metallicity ( $Z = 0.012$ ). All eight modes of the other four models were found to be excited.

The high metallicity ( $Z = 0.028$ ) of Model 2 (where  $f_1$  is the radial fundamental mode; “+” in Fig. 8) may also rule it out, since evidence points to  $\delta$  Ceti having a lower value of  $Z$  than this. Niemczura & Daszyńska-Daszkiewicz (2005) recently derived  $[m/H] = -0.24 \pm$

0.09 from UV iron transitions measured by IUE. Morel et al. (private communication) have derived the abundances of several important  $Z$ -determining elements from optical échelle spectra and found them to be only slightly less on average than solar values from Grevesse & Sauval (1998);  $Z = 0.02$ .

We conclude therefore that the dominant mode of  $\delta$  Ceti is the radial first overtone. Cugier et al. (1994) and Cugier & Nowak (1997) reached the same conclusion previously, but Daszyńska-Daszkiewicz et al. (2005) recently cast doubt on this identification, citing an excitation problem. Our non-adiabatic analysis shows that this mode is unstable for our Models 3, 4 and 5. Of these options, we prefer Model 3 because: (1) it is situated in the overlapping region of the photometric and spectroscopic error boxes, and (2) it has a metallicity ( $Z = 0.020$ ) consistent with values derived from high-quality spectra (whereas the other two models appear to be too metal-rich). The frequency  $f_2$  in this model is the  $g_2$   $\ell = 2$  mode.

#### 4.2. Multiplet structure in the $\delta$ Ceti eigenspectrum?

What of frequency  $f_3 = 3.673 \text{ d}^{-1}$ ? We note that it is separated from  $f_2$  by  $\Delta f = 0.064 \text{ d}^{-1}$ . If  $f_3$  is part of a rotationally-split multiplet, then there should be another sidelobe frequency at  $f_2 + \Delta f = 3.801 \text{ d}^{-1}$ . Note that we did find a peak in the MOST data at a frequency of  $3.805 \text{ d}^{-1}$  but with a significance of only  $2.8\sigma$ .

If  $f_2$  and  $f_3$  are consecutive  $m$ -values ( $\Delta m = 1$ ) of the same  $\ell = 2$  quintuplet, and we adopt the Ledoux coefficient  $\beta_{-2,2} = 0.85$  and radius of Model 3, we obtain a rotational frequency of  $0.075 \text{ d}^{-1}$  and an equatorial rotation velocity of  $27.6 \text{ km s}^{-1}$ . If they are separated by  $\Delta m = 2$ , then we derive half these values.

If we combine these values with the well measured value of  $v \sin i = 1 \pm 1 \text{ km s}^{-1}$  (Aerts et al. 1992), the inclination angle of  $\delta$  Ceti may be as small as  $i = 2^\circ$  (and cannot be larger than  $i = 8^\circ$ ). Hence we must be observing the star nearly pole-on. This conclusion is independent of the choice of models in Table 2.

The pole of a star corresponds to an angle of complete cancellation for an  $\ell = 2$  sectoral and tesseral mode (Chadid et al. 1999, their Table A.1). It is therefore most likely that  $f_2$  corresponds to the central peak of the quintuplet, as assumed in the modeling. Even if it were the outermost component of the quintuplet, the central peak would differ only by  $\simeq 0.13 \text{ d}^{-1}$  from  $f_2$ . Such a frequency shift is not large enough to affect our model identifications which assumed a low rotation rate and hence, closely spaced multiplet structure.

We also called attention in Sect. 3.3 to another frequency, at  $3.909 \text{ d}^{-1}$ , with a significance of  $3.5\sigma$ . This frequency would not fit into an equidistant quintuplet structure which includes  $f_2$  and  $f_3$ . We do note that Model 3 has a  $g_3 \ell = 3$  mode predicted to be excited whose frequency is close to  $3.909 \text{ d}^{-1}$ .

Finally, we have no obvious explanation for frequency  $f_4 = 0.318 \text{ d}^{-1}$ , but we do point out that  $f_4 \simeq 5(f_2 - f_3) \simeq 3(3.909 - 3.805) \text{ d}^{-1}$ , within the errors. Perhaps it is related to beating between modes.

## 5. Summary

MOST photometry of the  $\beta$  Cephei star  $\delta$  Ceti – until now regarded as a prototypical example of a monop periodic radial oscillator within the class – reveals the presence of at least two additional oscillations consistent with non-radial modes, as well as the first harmonic of the dominant radial mode. We have compared the new frequency spectrum with pulsation models constrained by stellar parameters based on photometric colors and spectroscopic analysis. We conclude that the dominant mode in  $\delta$  Ceti is due to the radial first overtone, and that the next strongest mode is the  $g_2 \ell = 2$  mode. We investigated multiplet structure associated with the latter mode to constrain the rotational velocity of the star, and showed that  $\delta$  Ceti is seen nearly pole-on.

We also find a shallow linear brightness increase in the star, at a rate of about  $0.0064 \text{ mmag/hour}$ . Jerzykiewicz et al. (1988) also found a drift in their *ubvy* photometry of  $\delta$  Ceti, but at a rate of about  $1 \text{ mmag/hour}$ . If both trends were truly intrinsic to the star, then the rate of brightness change would be strongly variable as a function of epoch. Such variations would not be surprising for an evolved star like  $\delta$  Ceti undergoing small instabilities on its way to the end of the central hydrogen burning phase. However, it is still possible that the trend seen by Jerzykiewicz et al. (1988) was an uncorrected effect of extinction in the Earth’s atmosphere. MOST does not suffer such extinction effects in orbit, but as a non-differential experiment, it is impossible to exclude an instrumental origin for the gradual trend it measured.

We note that Jerzykiewicz et al. (1988) also observed amplitude modulation in their night-to-night photometry which they suggested might be due to a second short-period variation with an amplitude below  $1.6 \text{ mmag}$ . The detection by MOST of frequency  $f_2$ , with an amplitude of about  $0.5 \text{ mmag}$  is consistent with that explanation.

The best model fit indicates that  $\delta$  Ceti has a mass of  $M = 10.2 \pm 0.2 M_\odot$ , an age of  $17.9 \pm 0.3$  million years and core overshooting ( $\alpha_{\text{ov}} = 0.20 \pm 0.05$ ). It is only the third

$\beta$  Cephei star for which the core overshooting parameter could be determined, along with HD 129929 ( $\alpha_{\text{ov}} = 0.10 \pm 0.05$ , Aerts et al. 2003) and  $\nu$  Eridani ( $\alpha_{\text{ov}} < 0.13$ , Pamyatnykh et al. 2004). The determination of the core overshooting parameter results in an accurate seismic mass estimate, which is for all three stars an improvement by an order of magnitude over previous photometric or spectroscopic mass estimates.

These results illustrate the power of nearly continuous ultra-precise photometry in understanding the structure and evolution of  $\beta$  Cephei stars. We can anticipate additional results from the space-based observatories WIRE (Brüntt et al., in preparation), MOST, COROT and Kepler in the coming years.

CA is indebted to Peter De Cat, Richard Scuflaire, Marc-Antoine Dupret and Mario Ausseloos for the use of their software. CA is supported by the Research Council of the K.U.Leuven under grant GOA/2003/04. SM acknowledges financial support from the Kentucky Space Grant Consortium. JMM, DBG, AFJM, SR and GAHW acknowledge funding from the Natural Sciences & Engineering Research Council (NSERC) Canada. RK’s work is supported by the Canadian Space Agency.

## REFERENCES

- Aerts, C., De Cat, P., Handler, G., et al. 2004, MNRAS 347, 436
- Aerts, C., De Pauw, M., Waelkens, C. 1992, A&A 266, 294
- Aerts, C., Thoul, A., Daszyńska, J., et al. 2003, Sci 300, 1926
- Ausseloos, M., Scuflaire, R., Thoul, A., Aerts, C. 2004, MNRAS 355, 352
- Ausseloos, M. 2005, PhD Thesis, Katholieke Universiteit Leuven, Belgium
- Breger, M., Stich, J., Garrido, R., et al. 1993, A&A 271, 482
- Briquet, M., Lefever, K., Uytterhoeven, K., Aerts, C. 2005, MNRAS 362, 619
- Brüntt, H., Buzasi, D.L. 2005, A&A, in preparation
- Chadid, M., De Ridder, J., Aerts, C., Mathias, P. 2001, A&A 375, 113
- Cugier, H., Dziembowski, W.A., Pamyatnykh, A.A. 1994, A&A 291, 143
- Cugier, H., Nowak, D. 1997, A&A 326, 620

- Daszyńska-Daszkiewicz, J., Dziembowski, W. A., Pamyatnykh, A.A. 2005, A&A 441, 641
- De Ridder, J., Telting, J., Balona, L.A., et al. 2004, MNRAS 351, 324
- Dupret, M.-A., 2001, A&A 366, 166
- Gies, D.R., Lambert, D.L. 1992, ApJ 387, 673
- Grevesse, N., Sauval, A.J. 1998, SSRv 85, 161
- Handler, G., Jerzykiewicz, M., Rodríguez, E., et al. 2006, MNRAS, in press
- Handler, G., Shobbrook, R.R., Jerzykiewicz, M., et al. 2004, MNRAS 347, 454
- Handler, G., Shobbrook, R.R., Mokgwetsi, T. 2005, MNRAS 362, 612
- Heynderickx, D., Waelkens, C., Smeyers, P. 1994, A&AS 105, 447
- Jerzykiewicz, M., Sterken, C., Kubiak, M. 1988, A&AS 72, 449
- Kubiak, M., Seggewiss, W. 1990, Acta Astron. 40, 85
- Kuschnig, R., Weiss, W. W., Gruber, R., et al. 1997, A&A 328, 544
- Montgomery, M.H., O'Donohue, D. 1999, Delta Scuti Newsletter 13, 28
- Morel, Th., Butler, K., Briquet, M., Neiner, C., Aerts, C. 2006, in preparation
- Niemczura, E., Daszyńska-Daszkiewicz, J. 2005, A&A 433, 659
- Pamyatnykh, A.A., Handler, G., Dziembowski, W.A. 2004, MNRAS 350, 1022
- Perryman, M.A.C., Lindegren, L., Kovalevsky, J. 1997, A&A 323, L49
- Reegen, P., Kallinger, T., Frast, D., et al., 2005, MNRAS, submitted
- Scargle, J.D. 1982, ApJ 263, 835
- Stankov, A., Handler, G. 2005, ApJS 158, 193
- Walker, G., Matthews, J., Kuschnig, R., et al. 2003, PASP 115, 1023

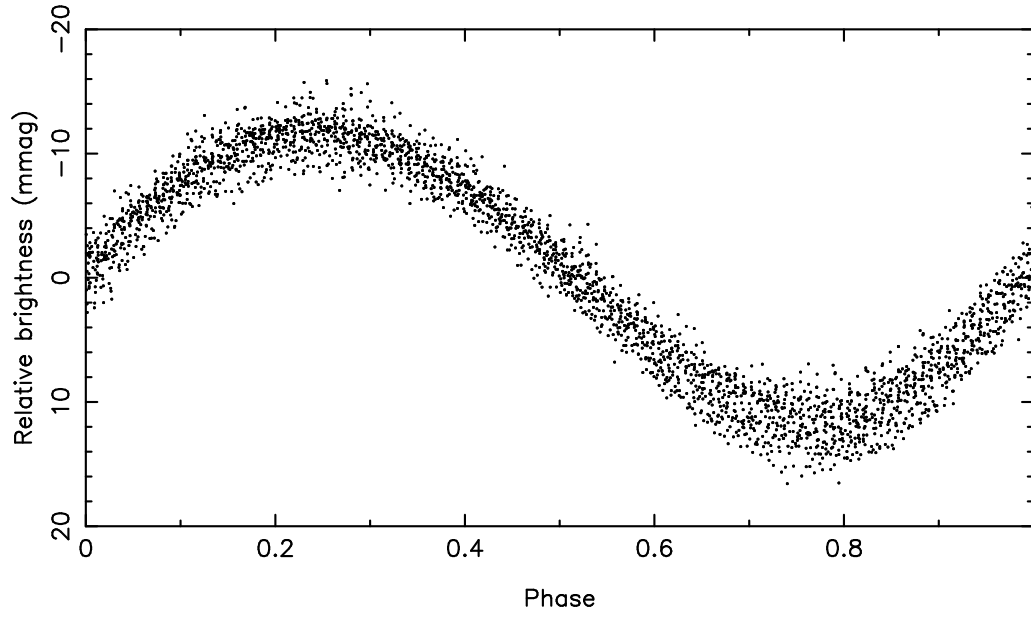


Fig. 1.— Phase diagram of the MOST data of  $\delta$  Ceti folded at the known dominant pulsation period of 0.161138 days



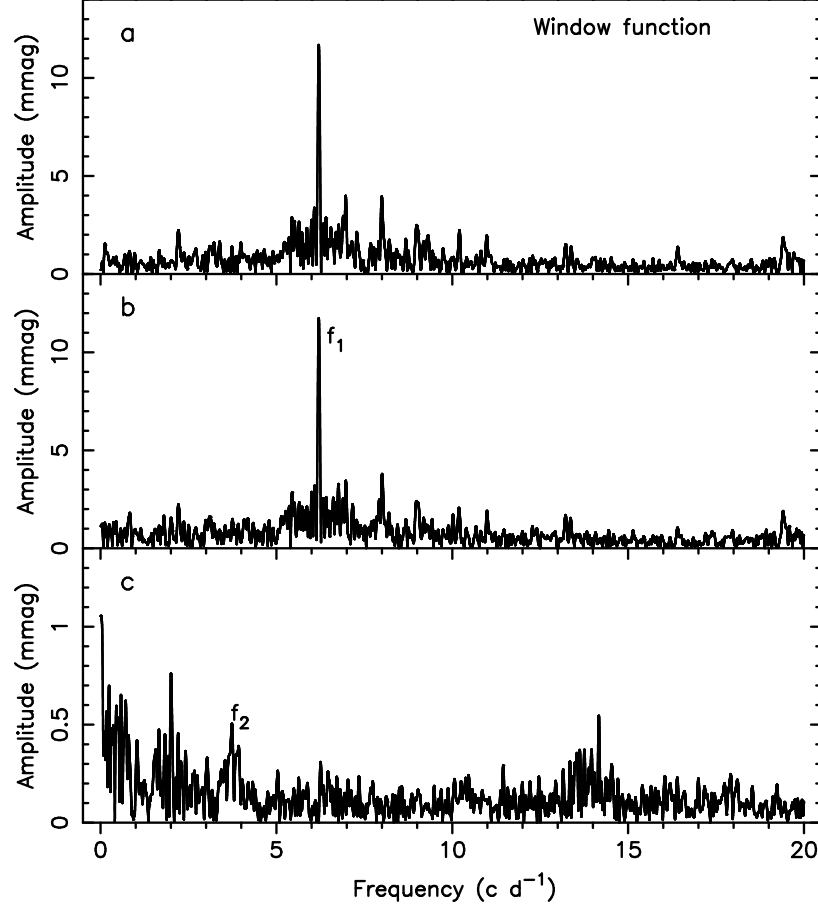


Fig. 2.— Periodograms of the MOST photometry of  $\delta$  Ceti. Panel a: window function shifted and scaled to the main peak; panel b: periodogram of the data; panel c: periodogram after prewhitening with  $f_1$  and  $2f_1$ .

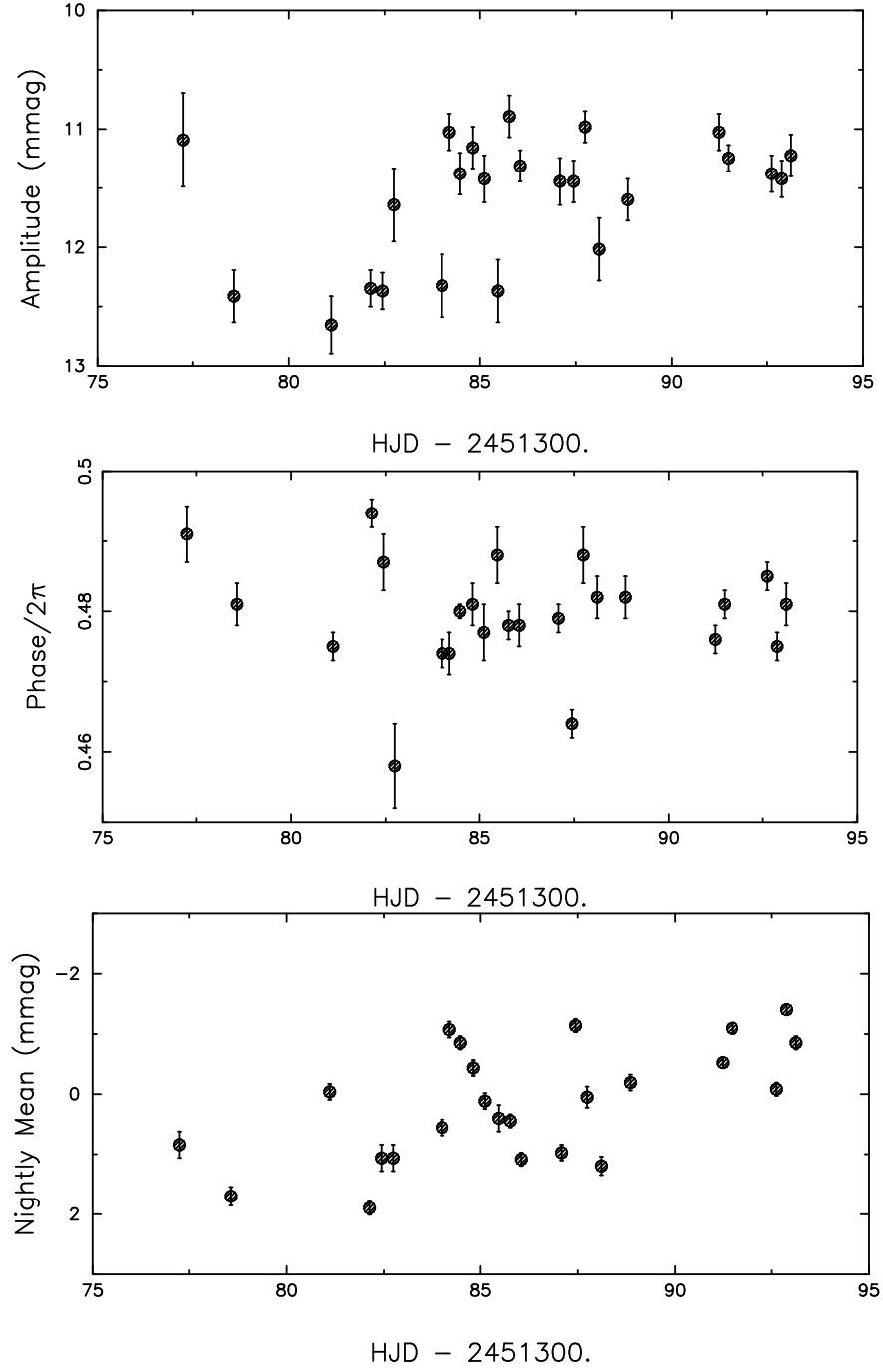


Fig. 3.— Amplitude of  $f_1$ , phase of  $f_1$  and mean with respect to the overall mean, for 25 datastrings observed by MOST.

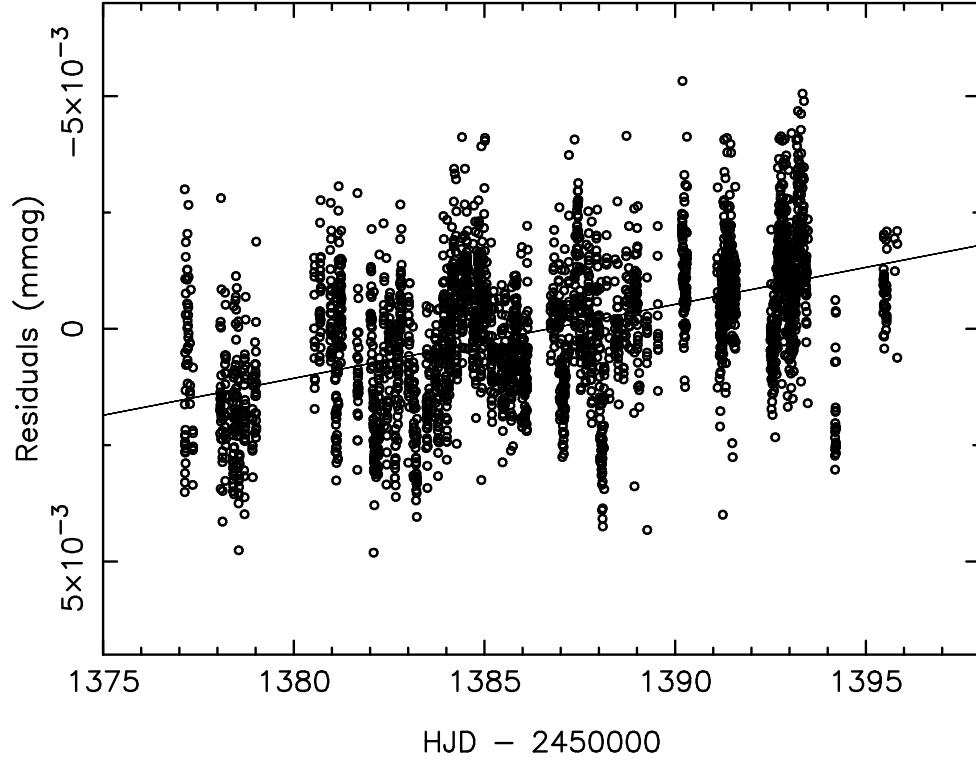


Fig. 4.— Brightness increase of  $\delta$  Ceti in the residuals after prewhitening the dominant frequency  $f_1$  and its harmonic from the MOST lightcurve.

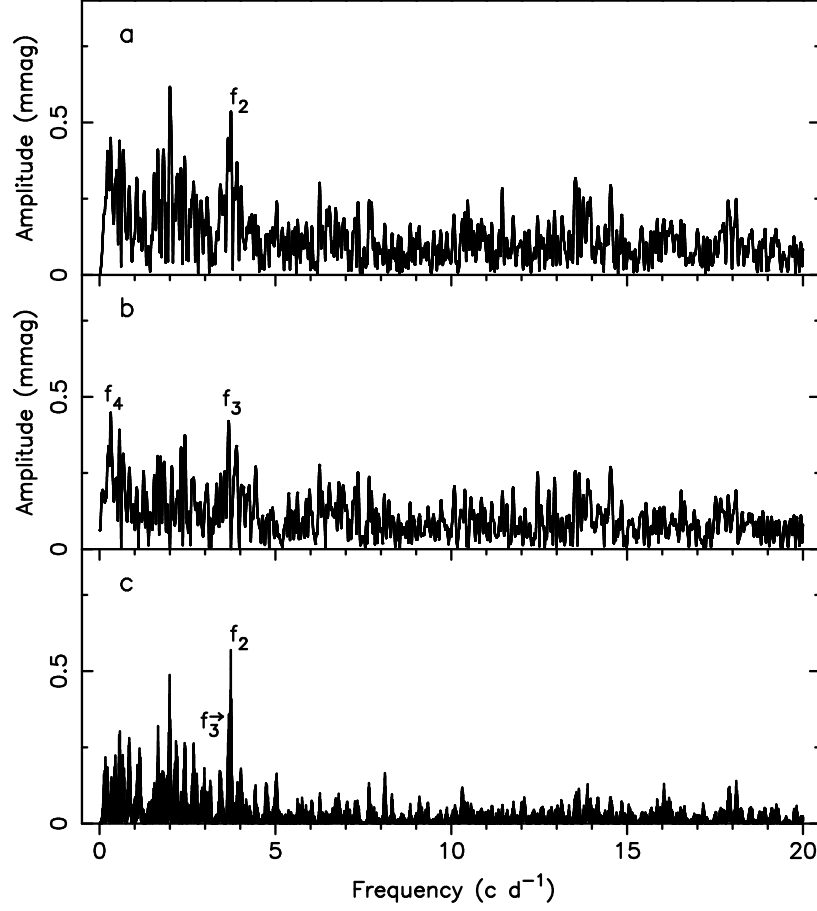


Fig. 5.— Periodograms of  $\delta$  Ceti. Panel a: after prewhitening with  $f_1$  and  $2f_1$  and detrending according to Fig. 4. Panel b: after subsequent prewhitening with  $f_2$  and  $2.003 \text{ d}^{-1}$ . Panel c: product of normalised amplitude spectra of the MOST and HIPPARCOS photometry and the first velocity moment  $\langle v \rangle$  taken from Aerts et al. (1992).

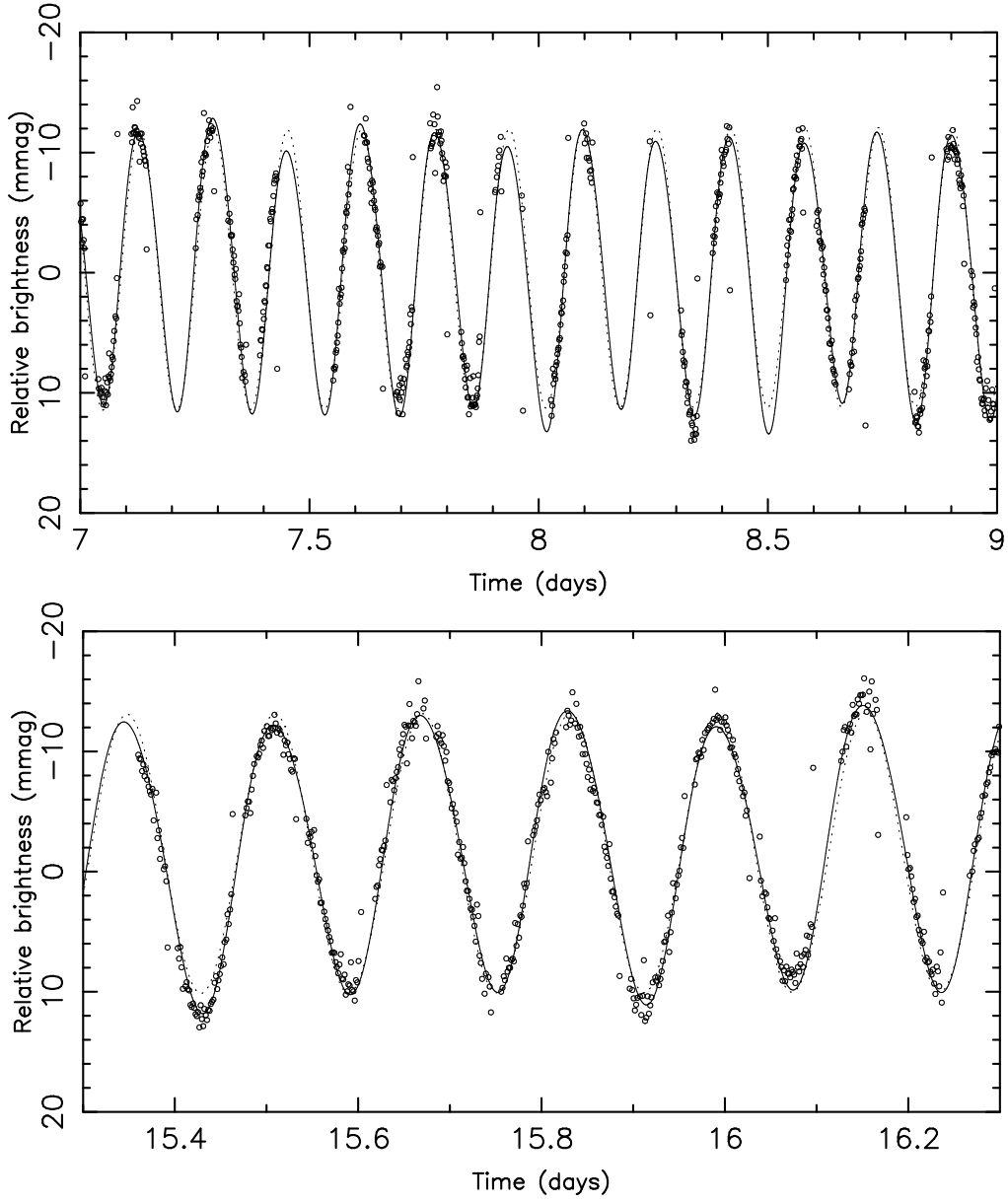


Fig. 6.— Comparison between the MOST data and (1) the final fit given in Eq.(1) (full line), (2) a fit including only the dominant frequency and the trend (dotted line) for a few selected segments.

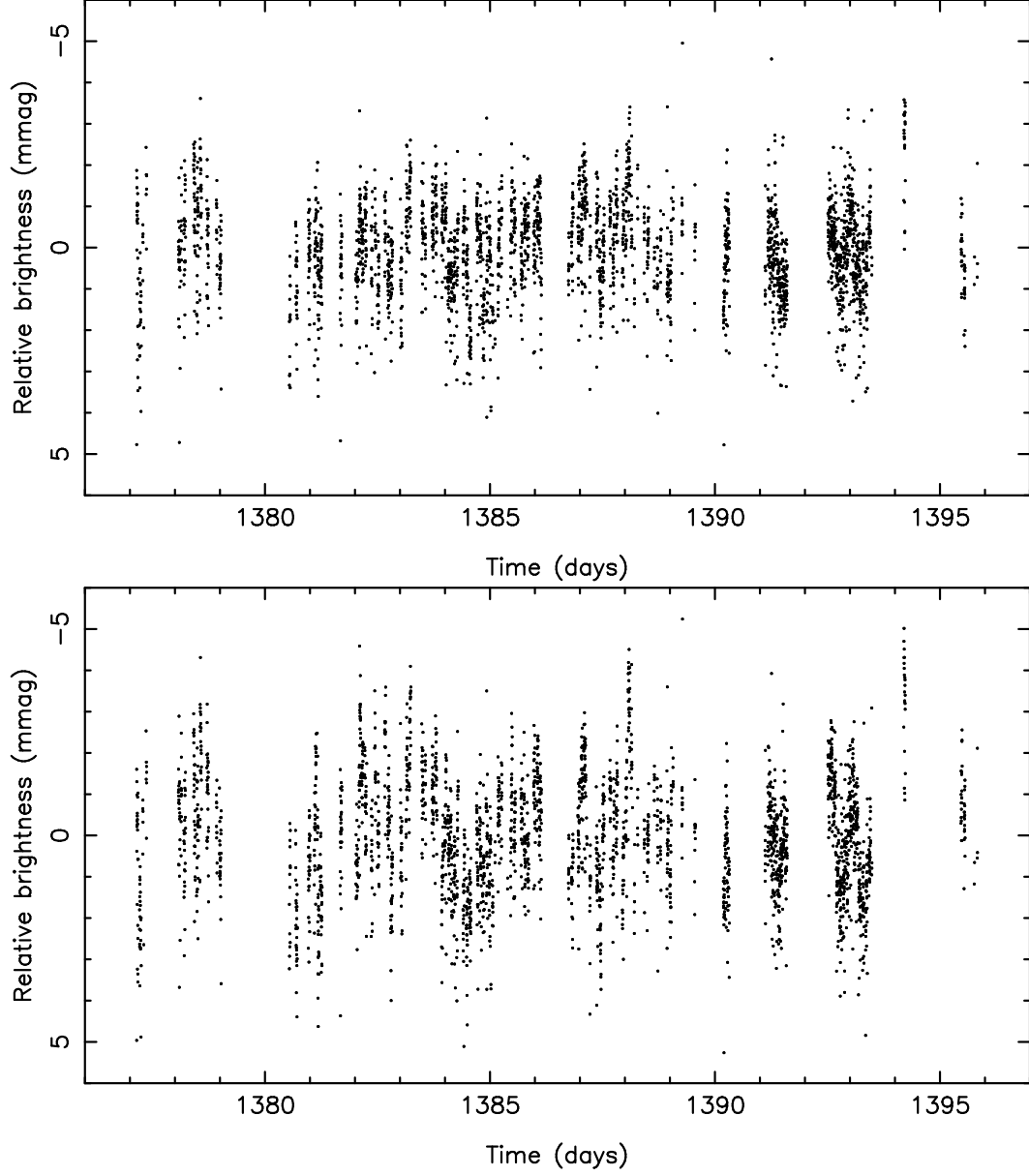


Fig. 7.— Residuals of the entire MOST data set after prewhitening by the final fit given in Eq. (1) (upper panel) and by only the dominant frequency  $f_1$  and the linear trend in the data (lower panel). The standard deviations of these residuals are 1.18 and 1.47 mmag, respectively.

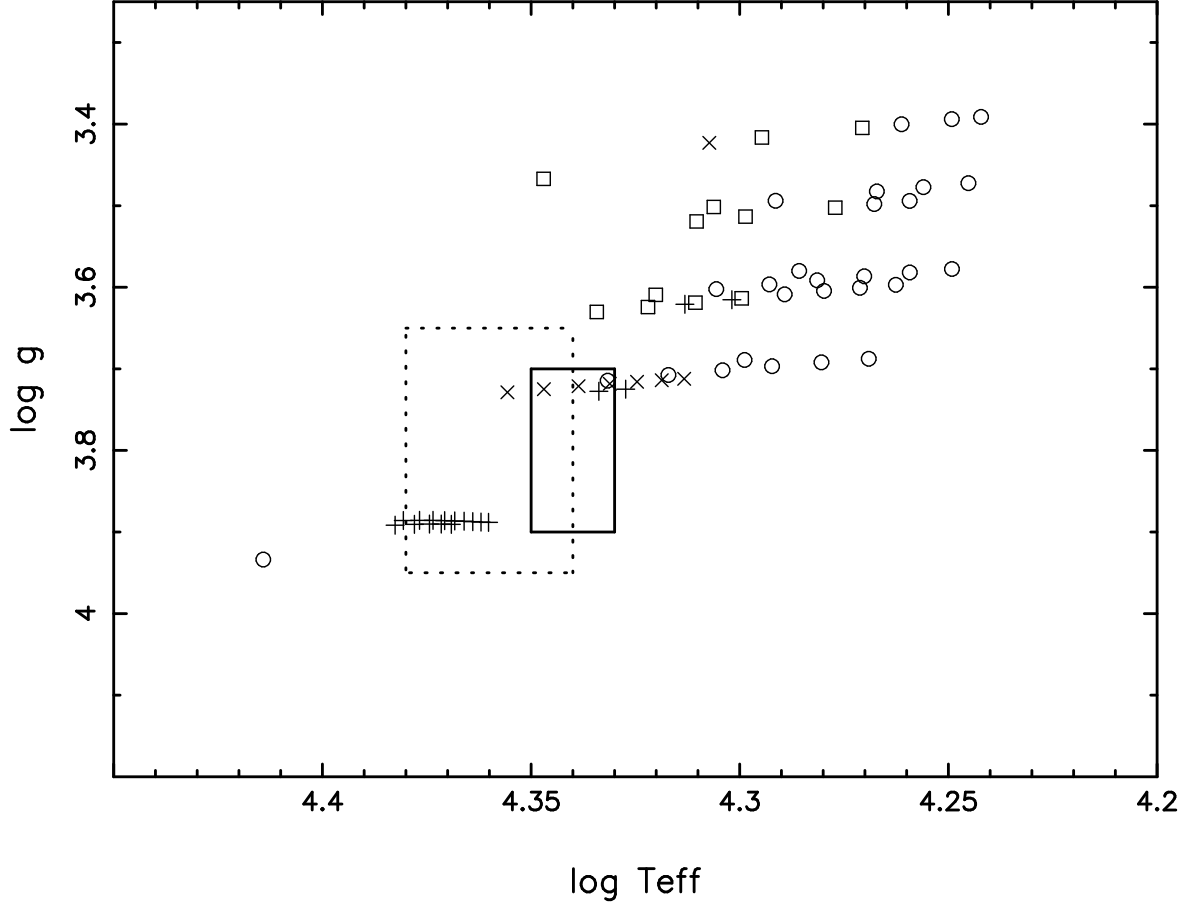


Fig. 8.— Position of stellar models in the  $(\log T_{\text{eff}}, \log g)$  diagram whose zonal modes fit  $f_1$  and  $f_2$  simultaneously. The symbol convention is as follows:  $f_1$  radial first overtone and  $f_2$  an  $\ell = 1, m = 0$   $g$  mode ( $\circ$ ),  $f_1$  radial second overtone and  $f_2$  an  $\ell = 1, m = 0$   $g$  mode ( $\square$ ),  $f_1$  radial fundamental and  $f_2$  an  $\ell = 2, m = 0$   $g$  mode ( $+$ ),  $f_1$  radial first overtone and  $f_2$  an  $\ell = 2, m = 0$   $g$  mode ( $\times$ ). The photometric (full lines) and spectroscopic (dotted lines) observational error boxes of  $\delta$  Ceti are also indicated.

Table 1. Final lightcurve solution of  $\delta$  Ceti, according to the eight terms given in Eq. (1).  
The reference epoch for the phases  $\phi_j$  is the time of the first measurement  
(HJD 2451377.140428).

$f_j$ (c d <sup>-1</sup> )	$f_j$ ( $\mu$ Hz)	$c_j$ (mmag)	$\phi_j$	S/N
$f_1 = 6.20589(8)$	71.8274(9)	11.62(3)	0.4958(4)	121.4
$2f_1$	$2f_1$	0.72(3)	0.619(7)	7.5
2.003(1)	23.18(1)	0.65(3)	0.292(7)	6.8
$f_2 = 3.737(2)$	43.25(2)	0.53(3)	0.454(9)	5.5
$f_3 = 3.673(2)$	42.51(2)	0.39(4)	0.82(1)	4.0
$f_4 = 0.318(2)$	3.68(2)	0.43(4)	0.55(2)	4.5
$a = 922.89(5)$ mmag				
$b = -0.154(5)$ mmag/day				



Table 2. Physical parameters of the stellar models within the photometric error box of  $\delta$  Ceti shown in Fig. 8. The core overshoot parameter is expressed in units of the local pressure scale height.

	$\log L/L_{\odot}$	$\log T_{\text{eff}}$	$\log g$	$M(M_{\odot})$	$R(R_{\odot})$	$X_c$	$X$	$Z$	$\alpha_{\text{ov}}$	age(yr)
1:○	3.977	4.332	3.714	9.43	7.06	0.088	0.70	0.012	0.0	$19.7 \times 10^6$
2:+	4.014	4.334	3.727	10.36	7.29	0.252	0.70	0.028	0.1	$16.9 \times 10^6$
3:×	4.064	4.347	3.725	10.23	7.27	0.249	0.70	0.020	0.2	$17.9 \times 10^6$
4:×	4.026	4.339	3.721	10.04	7.23	0.255	0.70	0.022	0.2	$18.6 \times 10^6$
5:×	3.992	4.331	3.718	9.88	7.20	0.260	0.70	0.024	0.2	$19.3 \times 10^6$